Computers and Mathematics with Applications 64 (2012) 1636–1648

Contents lists available at SciVerse ScienceDirect

Computers and Mathematics with Applications

journal homepage: www.elsevier.com/locate/camwa

A numerical study of the arc-roof and the one-sided roof enclosures based on the entropy generation minimization

Behrooz M. Ziapour *, Resam Dehnavi

Department of Mechanical Engineering, University of Mohaghegh Ardabili, Ardabil, Iran

ARTICLE INFO

Article history:
Received 17 June 2011
Received in revised form 31 December 2011
Accepted 3 January 2012

Keywords:
Entropy
Enclosure
Explicit
Finite-volume method
Greenhouse
Natural convection

ABSTRACT

This paper describes an enhanced finite-volume method for solving the arc-roof and the one-sided roof enclosures. Enclosures were assumed like two-dimensional cavities with the natural convection of air inside them. Various boundary conditions such as the greenhouse boundary conditions were considered. In order to estimate exergy destruction inside enclosures, the volumetric entropy generation in flow due to the heat transfer and the fluid friction was calculated using an enhanced scheme for finding the first derivative terms. In provided FORTRAN code, an explicit fourth-order Runge–Kutta integration algorithm was applied to find the steady state solutions. Next, the results were evaluated with other cited works. Also, performance of the one-sided roof enclosure was compared with the performance of the arc-roof enclosure based on their exergy destruction. Results showed that the entropy generation into the one-sided-roof type is less than the other.

1. Introduction

Natural convection in enclosures is a kind of classical problem in heat transfer. The shape of the wall, flow and heat transfer inside enclosures have numerous engineering applications such as heat exchangers, energy-storage devices, solar-collectors, greenhouses, double-wall insulation, electric machinery, cooling system of electronic devices, natural circulation in the atmosphere, etc. [1–6]. One important example of these applications is greenhouses. A greenhouse is an enclosed structure similar to enclosure, which traps the short wavelength solar radiation and stores the long wavelength thermal radiation to create a favorable microclimate for higher productivity [7]. In recent years, closed greenhouses have been investigated to reduce the summer ventilation and winter heating losses [8]. Therefore a greenhouse can be considered as solar collectors and their performance can be described in a similar way, in which the soil was considered as an absorber plate; the plants, as a semi-transparent medium, and the greenhouse cover was considered as the collector cover [9]. The several analytical and numerical approaches and techniques were conducted to obtain thermal characteristics of the greenhouses, by researches [10–13]. Also selection and optimization greenhouses based on the energy conservation have been performed [14–16]. It is seen that the literature about exergy performance of a greenhouse is surprisingly scarce.

The exergy analysis based on the second law of thermodynamics calculates exergy destruction of processes and has an important role in energy conversion systems. The optimal design criteria for thermal systems by minimizing their entropy generation have recently been a topic of great interest. Especially, in the fields related to geometry of a duct, natural convection in enclosure has gained the attraction of many researchers [17–19]. An important reason for this is the development of Computational Fluid Dynamics (CFD) which has not only made possible the analysis of several complex problems in thermal engineering but has also helped us in evaluating alternate designs quickly and efficiently.

In this work, by provided FORTRAN code, an enhanced explicit finite-volume procedure is presented for solving the natural convection of the laminar air flow in the arc-roof and the one-sided roof enclosures [1,20,21]. For enclosures, various

* Corresponding author. Tel.: +98 451 5512910; fax: +98 451 5512904.
E-mail address: behrooz_m_ziapour@yahoo.com (B.M. Ziapour).

0898-1221/$ – see front matter © 2012 Elsevier Ltd. All rights reserved.
doi:10.1016/j.camwa.2012.01.012

Nomenclature

A_G	the projected area of the cover on the horizontal plan, ground area, m
A_{Roof}	roof area, m
arc	ratio of the arc-roof radius to the enclosure height (arc $= r/h$)
Be	Bejan non-dimensional number, $Be = \dot{S}_{l,a,k}/\dot{S}_{l,a}$
C_p	specific heat at constant pressure, J/kg K
F	flow components vector
G	flow components vector
g	gravitational acceleration, m/s^2
h	enclosure height, characteristic length, m
H	dimensionless enclosure height, $H = 1$
k	thermal conductivity, W/m K
l	enclosure length, m
L	dimensionless enclosure length, $L = l/h$
p	static pressure, Pa
P	dimensionless static pressure, $P = ph^2/(\rho\alpha^2)$
Pr	Prandtl number
q	transmitted solar energy into the greenhouse enclosure per unit area of the cover surface, W/m^2
Q	flow components vector
$\dot{Q}_{\text{Solar}}$	total solar energy rate absorbed by the enclosure inner materials (plants, soil, cover and internal structures), W
$\dot{Q}_{\text{Loss},G}$	total loss energy rate from the ground, W
$\dot{Q}_{\text{Loss,Roof}}$	total loss energy rate from the roof, W
R	flow components vector
Ra	Rayleigh number
r	arc-roof radius, m
S	area cell
$\dot{S}$	entropy generation, W/m^3 K
t	time, s
T	temperature, K
T_c	constant cold wall temperature, K
T_h	constant hot wall temperature, K
u, v	velocity components in x, y direction, m/s
U, V	dimensionless velocity, components in x, y direction, $U = u/h$, $V = v/h$
W	flow components vector
x, y	Cartesian coordinates, m
X, Y	dimensionless Cartesian coordinates, $X = x/h$, $Y = Y/h$
Z	flow components vector

Greek letters

α	slope angle, thermal diffusivity, m^2/s
β	artificial compressibility parameter
Δ	distance, m
μ	dynamic viscosity, kg/m s
υ	kinematics viscosity, m^2/s
ρ	density, kg/m^3
ζ	dimensionless time
φ	ratio between the viscous and thermal irreversibilities
θ	dimensionless temperature, $\theta = (T - T_c)/(T_h - T_C)$

Subscripts

a	dimensionless
arc	arc of roof
c	cold
Earth	earth
h	heat transfer effect, hot
f	fluid viscous effect
G	ground

House	inside of greenhouse
i, j	selected cell in order to analyze
l	local
Loss	energy loss
Max	maximum
Min	minimum
Soil	soil
T	total
W	wall
∞	ambient
Ω	selected control volume in order to analyze
$\delta\Omega$	bound of the control volume

boundary conditions such as the greenhouse boundary conditions were considered. For each greenhouse enclosure, the conjugate boundary conditions were considered. Also the greenhouses were evaluated based on the entropy generation inside them.

In this work, an artificial compressibility technique is applied to couple the continuity to the momentum equations. This technique was originally introduced by Chorin with the objective of solving the steady state incompressible Navier–Stokes equations. Chorin transformed the elliptic incompressible equations to a hyperbolic compressible system, which can be solved by standard, time-marching methods. The idea of relaxing the incompressibility constraint by adding an artificial compressibility term has been known for a long time and has been extensively used in finite-volume as well as in finite element approximations of the incompressible Navier–Stokes equations [22–25].

In this work, the discretization of the viscous and thermal conduction terms are very simplified using the enhanced scheme similar to flux averaging in the convective terms. Recently, this enhanced method has been introduced by Ziapour and Dehnavi (see Ref. [1]). In this new method, the terms of the volumetric entropy generation in flow (i.e. the first order derivatives as: $\partial\theta/\partial X$, $\partial\theta/\partial Y$, $\partial U/\partial X$, $\partial U/\partial Y$, $\partial V/\partial X$ and $\partial V/\partial Y$) in the form of functions are initially guessed, and then are corrected after the each time step through the time marching processes.

2. Governing equations

The two-dimensional incompressible viscous flow governing equations in non-dimensional form and with artificial compressibility can be written as follows [1]:

$$\frac{1}{\beta}\frac{\partial P}{\partial \zeta} + \frac{\partial U}{\partial X} + \frac{\partial V}{\partial Y} = 0 \tag{1}$$

$$\frac{\partial U}{\partial \zeta} + \frac{\partial (UU)}{\partial X} + \frac{\partial (UV)}{\partial Y} = -\frac{\partial P}{\partial X} + \frac{\partial}{\partial X}\left(Pr\frac{\partial U}{\partial X}\right) + \frac{\partial}{\partial Y}\left(Pr\frac{\partial U}{\partial Y}\right) \tag{2}$$

$$\frac{\partial V}{\partial \zeta} + \frac{\partial (UV)}{\partial X} + \frac{\partial (VV)}{\partial Y} = -\frac{\partial P}{\partial Y} + \frac{\partial}{\partial X}\left(Pr\frac{\partial V}{\partial X}\right) + \frac{\partial}{\partial Y}\left(Pr\frac{\partial V}{\partial Y}\right) + PrRa\theta \tag{3}$$

$$\frac{\partial \theta}{\partial \zeta} + \frac{\partial (U\theta)}{\partial X} + \frac{\partial (U\theta)}{\partial Y} = \frac{\partial}{\partial X}\left(\frac{\partial \theta}{\partial X}\right) + \frac{\partial}{\partial Y}\left(\frac{\partial \theta}{\partial Y}\right) \tag{4}$$

where, U and V are dimensionless Cartesian velocity components; X and Y are dimensionless Cartesian axis; P is dimensionless static pressure; θ is dimensionless temperature; ζ is dimensionless time; Pr is Prandtl number; Ra is Rayleigh number; β is the artificial compressibility that is given as follows:

$$\frac{\partial \rho}{\partial t} = \frac{1}{\beta}\frac{\partial p}{\partial t}. \tag{5}$$

3. Formulation of the heat transfer characteristics

The volumetric entropy generation in flow due to the heat transfer and fluid friction can be written as follows [1]:

$$\dot{S}_l = \dot{S}_{l.h} + \dot{S}_{l.f}. \tag{6}$$

The heat transfer contribution of the volumetric entropy generation of the two-dimensional flow system is

$$\dot{S}_{l,h} = \frac{k}{T_0^2}\left[\left(\frac{\partial T}{\partial x}\right)^2 + \left(\frac{\partial T}{\partial y}\right)^2\right]. \tag{7}$$

The fluid friction contribution of the volumetric entropy generation of the two-dimensional flow system is as:

$$\dot{S}_{l.f} = \frac{\mu}{T_0}\left[2\left(\frac{\partial u}{\partial x}\right)^2 + 2\left(\frac{\partial v}{\partial y}\right)^2 + \left(\frac{\partial u}{\partial y} + \frac{\partial v}{\partial x}\right)^2\right]. \tag{8}$$

These dimensionless equations can be written as follows:

$$\dot{S}_{l.a} = \dot{S}_{l.a.h} + \dot{S}_{l.a.f} \tag{9}$$

$$\dot{S}_{l.a.h} = \left[\left(\frac{\partial \theta}{\partial X}\right)^2 + \left(\frac{\partial \theta}{\partial Y}\right)^2\right] \tag{10}$$

$$\dot{S}_{l.a.f} = \varphi\left[2\left(\frac{\partial U}{\partial X}\right)^2 + 2\left(\frac{\partial V}{\partial X}\right)^2 + \left(\frac{\partial U}{\partial Y} + \frac{\partial V}{\partial X}\right)^2\right] \tag{11}$$

where, φ is the ratio between the viscous and thermal irreversibilities as the following equation:

$$\varphi = \frac{\mu T_0}{k}\left[\frac{\alpha}{L(T_h - T_c)}\right] \tag{12}$$

where, $T_0 = (T_h + T_c)/2$ is the bulk temperature.

The dimensionless total entropy generation is the integral over the system volume of the dimensionless local entropy generation:

$$\dot{S}_{T.a} = \int \dot{S}_{l.a} dv. \tag{13}$$

4. Cell centered finite-volume scheme for space discretization

By integrating from conservation equations (1)–(4) over a control volume Ω, which is bounded by $\partial\Omega$, and applying the Gauss divergence theorem, one gets the following equations [1]:

$$\iint_\Omega \frac{1}{\beta}\frac{\partial P}{\partial \zeta} dS = -\oint_{\partial\Omega} (UdY - VdX) \tag{14}$$

$$\iint_\Omega \frac{\partial U}{\partial \zeta} dS = -\oint_{\partial\Omega} PdY - \int_{\partial\Omega} (U^2 dY - UVdX) + Pr\int_{\partial\Omega}\left(\frac{\partial U}{\partial X}dY - \frac{\partial U}{\partial Y}dX\right) \tag{15}$$

$$\iint_\Omega \frac{\partial V}{\partial \zeta} dS = \oint_{\partial\Omega} PdX - \int_{\partial\Omega} (UVdY - V^2 dX) + Pr\int_{\partial\Omega}\left(\frac{\partial V}{\partial X}dY - \frac{\partial V}{\partial Y}dX\right) + PrRa\theta\iint_{\partial\Omega} dS \tag{16}$$

$$\iint_\Omega \frac{\partial \theta}{\partial \zeta} dS = \int_{\partial\Omega}\left(\frac{\partial \theta}{\partial X}dY - \frac{\partial \theta}{\partial Y}dX\right) - \int_{\partial\Omega} (U\theta dY - V\theta dX). \tag{17}$$

Therefore, these equations can be arranged in the suitable vector form as follows:

$$\frac{\partial}{\partial \zeta}\iint_\Omega Q dS = -\oint_{\partial\Omega} (FdY - GdX) + \oint_{\partial\Omega} (RdY - Wdx) + \iint_\Omega Z dS \tag{18}$$

where Q, F, G, R, W and Z are the flow component vectors as the following definitions:

$$Q = \begin{pmatrix} P \\ U \\ V \\ \theta \end{pmatrix}, \quad F = \begin{pmatrix} \beta U \\ U^2 + P \\ UV \\ U\theta \end{pmatrix}, \quad G = \begin{pmatrix} \beta V \\ UV \\ V^2 + P \\ V\theta \end{pmatrix}, \quad R = \begin{pmatrix} 0 \\ Pr\dfrac{\partial U}{\partial X} \\ Pr\dfrac{\partial V}{\partial X} \\ \dfrac{\partial \theta}{\partial X} \end{pmatrix},$$
$$W = \begin{pmatrix} 0 \\ Pr\dfrac{\partial U}{\partial Y} \\ Pr\dfrac{\partial V}{\partial Y} \\ \dfrac{\partial \theta}{\partial Y} \end{pmatrix}, \quad Z = \begin{pmatrix} 0 \\ 0 \\ PrRa\theta \\ 0 \end{pmatrix}. \tag{19}$$

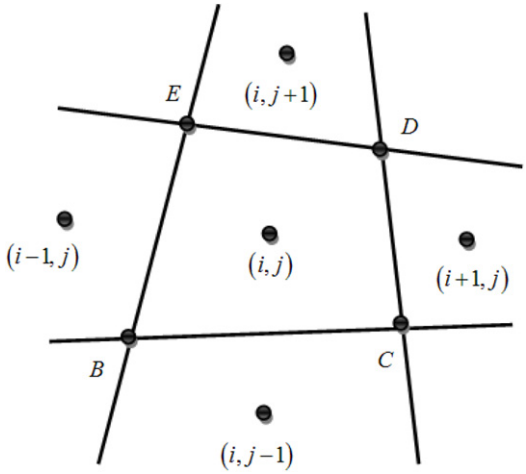

Fig. 1. Cells in the finite-volume approach.

The computational domain is divided into quadrilateral cells (see Fig. 1) and a system of ordinary differential equations is obtained by applying Eq. (18) to each cell separately.

In order to find the convective terms in the boundaries of the cell (i, j), we select the custom flux averaging scheme. In this scheme each quantity such as $(U\theta)_1$ (i.e. the value of $U\theta$ on the boundary denoted by number 1, as shown in Fig. 1), is evaluated as the average of the cells values, on either side of the face (i.e. $(U\theta)_1 = 1/2[(U\theta)_{i,j} + (U\theta)_{i,j-1}]$).

Here, the mentioned above flux averaging method is applied for the viscous and conduction terms (see Ref. [1]). In this new method, we need to know the first derivatives such as $(\partial\theta/\partial y)_{i,j}$ and so on (at the cell center). These functions are obtained from the Gauss divergence theorem. For example, we have $(\partial\theta/\partial y)_{i,j} = -1/S_{i,j} \oint_{\partial\Omega} \theta dx$. Therefore, these derivatives are saved for all cells as the functions that can be used in the next time step. For example, the value of $(\partial\theta/\partial y)_1$ is found as: $(\partial\theta/\partial y)_1 = 1/2[(\partial\theta/\partial y)_{i,j} + (\partial\theta/\partial y)_{i,j-1}]$.

After discretizing Eq. (18) around (i, j)th cell and to consider the cell centered assumption for variables, then the following equation results:

$$S_{i,j}\frac{\partial Q_{i,j}}{\partial \zeta} = -\sum_{k=1}^{4}(F_{i,j}\Delta Y - G_{i,j}\Delta X)_k + \sum_{k=1}^{4}(R_{i,j}\Delta Y - W_{i,j}\Delta X)_k + S_{i,j}Z_{i,j} \tag{20}$$

where, $S_{i,j}$ is the area of (i, j)th cell.

The first order derivatives of the viscous and conduction terms, obtained from flux averaging scheme are used for finding the algebraic form of entropy equation (9). By noticing Eqs. (10) and (11), it is seen that, in these equations, all terms are the first order derivatives of the flow components (i.e. $\partial\theta/\partial x$, $\partial\theta/\partial y$, $\partial U/\partial x$, $\partial U/\partial y$, $\partial V/\partial x$ and $\partial V/\partial y$). These derivatives were known in the prior computations for the diffusion terms. For example, we have the following algebraic form for Eqs. (10) and (11):

$$(\dot{S}_{l.a.h})_{i,j} = [(\partial\theta/\partial X)_{i,j}]^2 + [(\partial\theta/\partial Y)_{i,j}]^2 \tag{21}$$

$$(\dot{S}_{l.a.f})_{i,j} = \varphi\{2[(\partial U/\partial X)_{i,j}]^2 + 2[(\partial V/\partial X)_{i,j}]^2 + [(\partial U/\partial Y)_{i,j} + (\partial V/\partial X)_{i,j}]^2\}. \tag{22}$$

5. Results and discussions

5.1. Validation of the computational schemes

In order to find the steady state solution of the ordinary differential equation (20), an explicit fourth-order Runge–Kutta integration algorithm was applied. To find a grid free solution, different grid sizes, ranged 30×30, 50×50 and 100×100 (based on the $L \times H$ area) were tested. In this range, the difference between maximum value of the Bejan number (Be_{Max}) and its minimum value (Be_{Min}) was obtained, about 2%. Finally, 50×50 grid points are selected on the basis of less computation time and without compromising the grid dependence. Also, the convergence criterion was used for the mass conservation residue, established in 10^{-8}.

Fig. 2 shows the sample of the history of the mass conservation residues (Res) for different values of the artificial compressibility parameters (β). One can see that the good convergence speed obtains for β value as $\beta = 300$.

The boundary conditions, as shown in Fig. 3, were selected for the numerical scheme validations. The enclosure geometries changed to rectangular shapes in three stages. The trace lines of these changes have been shown with dash lines in Fig. 3. These final rectangular situations are similar to works of Oliveski et al. [2] and Famouri and Hooman [26]. We

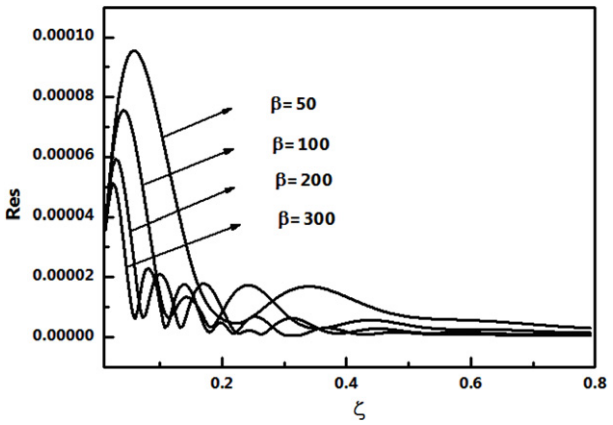

Fig. 2. The history of the mass conservation residues (Res) for different values of the artificial compressibility parameter (β).

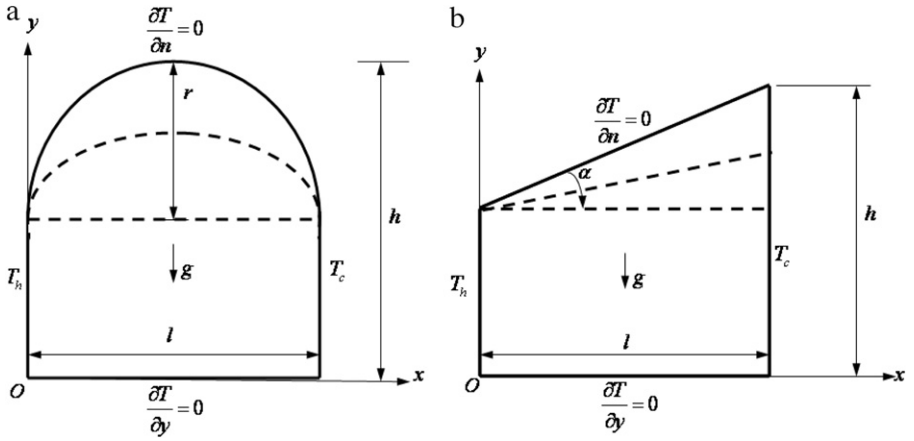

Fig. 3. The physical geometries and boundary conditions for the numerical process validation: (a) the arc-roof enclosure and (b) the one-sided roof enclosure.

Table 1
Validation of the entropy generation ($\dot{S}_{T,a}$) for the arc-roof enclosure.

	Oliveski et al. work [2] ($L = H = 1.0$)	Famouri and Hooman work [26] ($L = H = 1.0$)	Present work, (arc-roof)	Deviation (%)	
				Ref. [2]	Ref. [26]
$\dot{S}_{T,a}$ ($Ra = 10^3$)	4.557	4.558	4.068 (arc = 0.2)	10.73	10.75
	4.557	4.558	4.391 (arc = 0.1)	3.64	3.66
	4.557	4.558	4.559 (arc = 0.0)	0.04	0.02

Table 2
Validation of the entropy generation ($\dot{S}_{T,a}$) for one-sided roof enclosure.

	Oliveski et al. work [2] ($L = H = 1.0$)	Famouri and Hooman work [26] ($L = H = 1.0$)	Present work, (one-sided roof)	Deviation (%)	
				Ref. [2]	Ref. [26]
$\dot{S}_{T,a}$ ($Ra = 10^3$)	4.557	4.558	4.097 ($\tan\alpha = 0.2$)	10.09	10.11
	4.557	4.558	4.327 ($\tan\alpha = 0.1$)	5.05	5.06
	4.557	4.558	4.559 ($\tan\alpha = 0.0$)	0.04	0.02

listed the conducted results for values of $\dot{S}_{T,a}$ in Tables 1 and 2. According to deviation values, one can see that the results obtained from the present model are as good as they were expected.

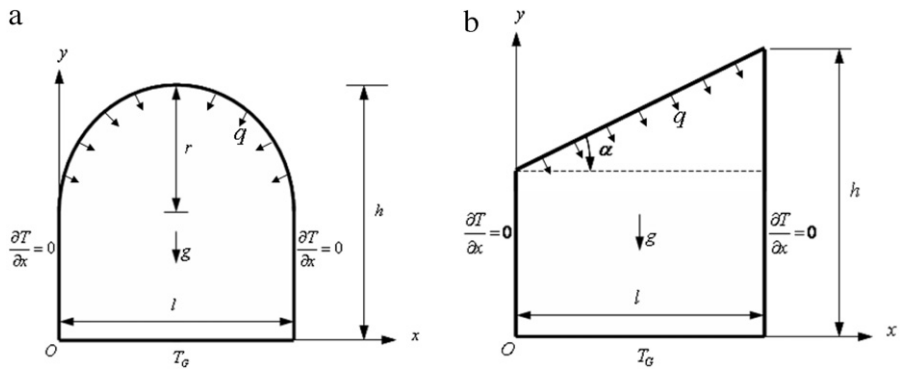

Fig. 4. The physical geometries and boundary conditions for the greenhouse situations: (a) the arc-roof enclosure and (b) the one-sided roof enclosure.

5.2. Greenhouse case study results

5.2.1. Applying the boundary conditions

The entered sun rays in a greenhouse can shine freely on the greenhouse floor, when the entropy generation reaches its lowest value; then, the process of photosynthesis will occur in the desired form. Finally, plants grow faster. The boundary conditions, as shown in Fig. 4a and b, simulate the arc-roof and the one-sided roof enclosures like greenhouses respectively. In these figures, it is assumed that the constant heat flux (q) is transmitted from the transparent cover roofs, due to the sun shine, and then is completely absorbed by the materials (plants, soil, cover and internal structures) inside them. It is assumed that both the plants and the soil make the greenhouses ground boundaries. Therefore, both the plants and the soil have identical temperature. According to these figures, the lateral walls are assumed as insulation. For the roofs and the grounds the conjugate boundary conditions are considered.

In this work, two kinds of boundary conditions are used: one for functions and another for their first order derivatives, as the following procedures.

(a) *For velocity components.*

It is assumed to be non-slipping in all cavity walls. Therefore under these assumptions, the dimensionless variables for velocity components at the greenhouse walls are obtained as: $U = V = 0$ (for all walls). Therefore their first dimensionless derivatives as: $\partial U/\partial X$, $\partial U/\partial Y$, $\partial V/\partial X$, $\partial V/\partial Y$ are linearly interpolated from the inner and vicinity of the boundary cells.

(b) *For temperatures.*

In the ground, we assumed the constant boundary conditions for temperatures (T_G). According to the convenient temperature that is needed for the growth of the plants, since we assumed the identical temperatures for soil and the plants, we can consider $18 \leq T_G \leq 23$. Therefore we have $\theta_G = (T_G - T_\infty)/(T_G - T_\infty) = 1$ as the dimensionless value for temperature at the ground. Therefore one of the first dimensionless derivatives is as $\partial\theta_G/\partial X = 0$ and another i.e. $\partial\theta_G/\partial Y$ is linearly interpolated from the inner and vicinity of the boundary cells.

In the lateral walls, we assumed the adiabatic condition. Therefore, we have $\partial\theta_W/\partial X = 0$. The other remainder variables are linearly interpolated from the interior cells near the wall.

In the transparent roof boundary, we assumed the constant heat flux (q). By referring to Figs. 5a and 6a, the energy balance between the entrance passive solar energy ($\dot{Q}_{\text{Solar}}$) and the heat losses energies via both the transparent roof ($\dot{Q}_{\text{Loss,Roof}}$) and the ground ($\dot{Q}_{\text{Loss},G}$), the following equation results:

$$\dot{Q}_{\text{Solar}} = \dot{Q}_{\text{Loss,Roof}} + \dot{Q}_{\text{Loss},G}. \tag{23}$$

In Eq. (23), the value of $\dot{Q}_{\text{Solar}}$ is as follows:

$$\dot{Q}_{\text{Solar}} = qA_{\text{Roof}} \tag{24}$$

where A_{Roof} is the roof area.

By referring to Figs. 5c and 6c, the value $\dot{Q}_{\text{Loss},G}$ is obtained from the following equation:

$$\dot{Q}_{\text{Loss},G} = -K_{\text{Soil}}A_G\frac{T_{\text{Earth}} - T_G}{\Delta_G} \tag{25}$$

where K_{Soil} is the moisture soil conductivity, A_G is the ground area and T_{Earth} is the average temperature of the earth at the depth of the Δ_G. In this work, we considered the values of the K_{Soil}, T_{Earth} and Δ_G as 2.5 (W/m^2 K), $T_G - 8$ and 0.4 (m)

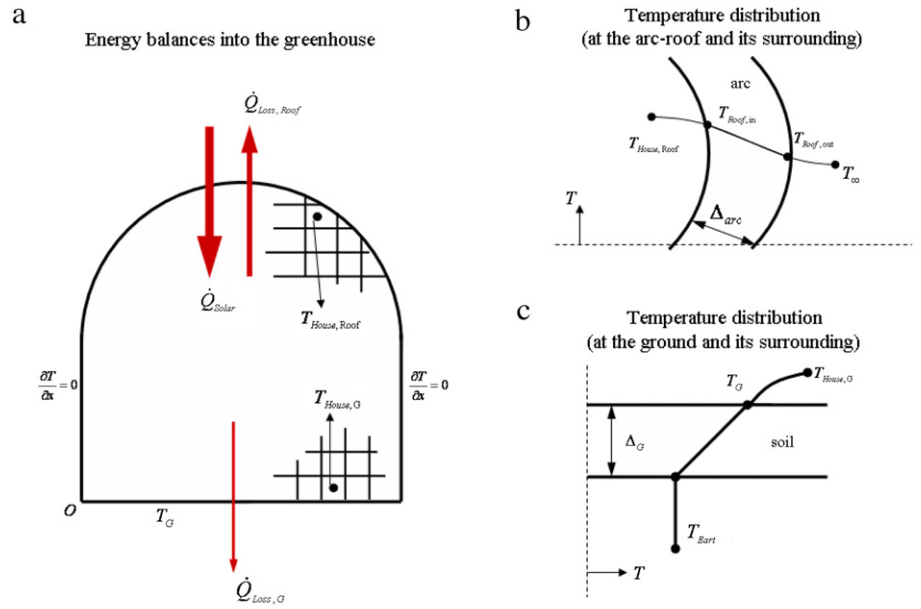

Fig. 5. The heat transfer characteristics of the arc-roof greenhouse: (a) energy balances, (b) temperature distribution at the arc-roof and (c) temperature distribution at the ground.

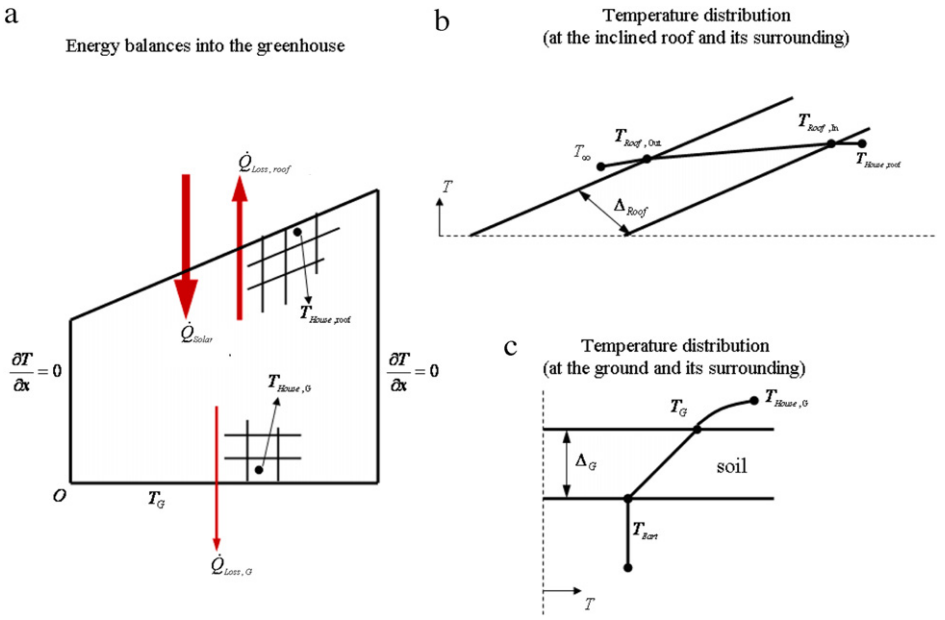

Fig. 6. The heat transfer characteristics for the one-sided roof greenhouse: (a) energy balances, (b) temperature distribution at the one-sided roof and (c) temperature distribution at the ground.

respectively. Therefore the value of $\dot{Q}_{Loss,G}$ is completely known. Thus the value of $\dot{Q}_{Loss,Roof}$ is known from Eq. (23). Also, by referring to Figs. 5b and 6b, the value of $\dot{Q}_{Loss,Roof}$ is related to the following equation as:

$$\dot{Q}_{Loss,Roof} = -K_{Roof}A_{Roof}\frac{T_{Roof,Out} - T_{Roof,In}}{\Delta_{Roof}} \tag{26}$$

where the values of the K_{Roof}, $T_{Roof,Out}$ and Δ_{Roof} are assumed to be the conductivity for glass, T_∞ and the roof thickness respectively. These values are the design parameters. In this work, the value Δ_{roof} is considered equal to 0.006 (m).

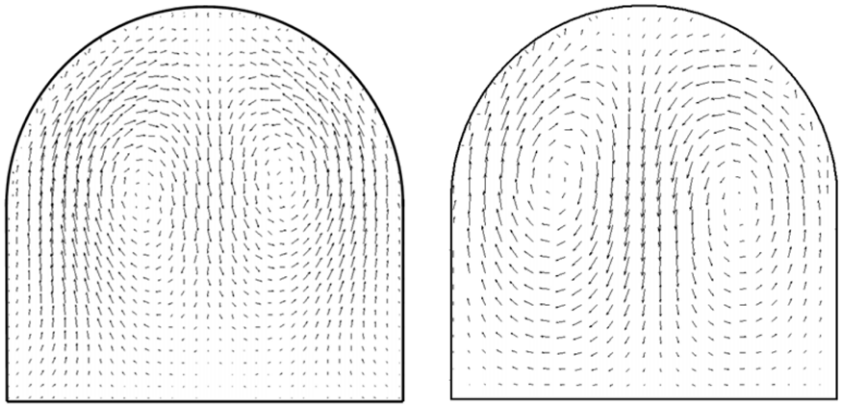

Fig. 7. Velocity fields for arc-roof greenhouse (with $L/H = 1$, arc $= 0.5$ and $T_G = 23$ °C), in two different ambient temperatures: (1) $T_\infty = 22$ °C (left figure) and (2) $T_\infty = 10$ °C (right figure).

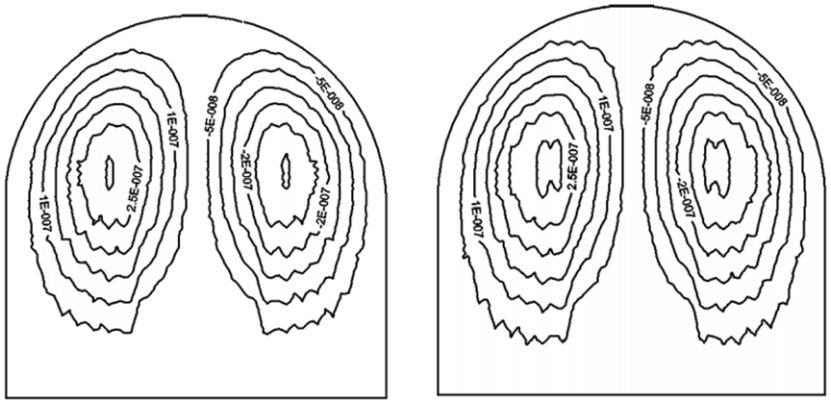

Fig. 8. Stream lines for arc-roof greenhouse (with $L/H = 1$, arc $= 0.5$ and $T_G = 23$ °C), in two different ambient temperatures: (1) $T_\infty = 22$ °C (left figure) and (2) $T_\infty = 10$ °C (right figure).

Also the value K_{Roof} has been considered as the conductivity for glass. Therefore the value $T_{\text{Roof,In}}$ is known. Thus, its dimensionless value (i.e. $\theta_{\text{Roof,in}} = (T_{\text{Roof,in}} - T_\infty)/(T_G - T_\infty)$) is known. Also its first derivative lineal value is directly obtained from Eq. (26).

For enclosures, the dimensionless Rayleigh number (Ra), is the criteria to distinguish the laminar flow from the turbulent flow regime. We checked Rayleigh number for greenhouse cases. In this test, all Rayleigh number values were obtained below 1000. Therefore the flow regime for this work is incompressible and laminar.

5.2.2. The arc-roof simulation results

Velocity fields have been shown in Figs. 7. Two figures have been sketched (with $L/H = 1$ and arc $= 0.5$), in two different ambient temperatures: (1) $T_\infty = 22$ °C (left figure) and (2) $T_\infty = 10$ °C (right figure). It reveals that, two approximately similar circulations (with opposite spin) are formed due to the free convection heat transfer mechanism. Also these stream lines have been plotted in Figs. 8. These figures prove that two approximately similar circulations (with opposite spin) are formed due to the free convection heat transfer mechanism.

For aspect ratio equal to 3 ($L/H = 3$) the isotherms and their stream lines have been shown in Fig. 9a–d. According to stream lines, two main circulations are revealed: one, the larger circulation cell on the left and the other, the weaker circulation cell on the right are formed in the greenhouse. According to isotherms, where the two vorticity zones are distinguished from each other, the isotherms exit from the straight and horizontal forms.

Fig. 10a–d, show the variation of the total entropy generation $\dot{S}_{T,a}$ vs. the ambient temperature T_∞, for different arc values (arc $= 0.4, 0.5, 0.6, 0.7, 0.8$). In all figures, the value of ground temperature is constant ($T_G = 23$ °C). It is seen that with the increase of T_∞, the $\dot{S}_{T,a}$ increases. As shown in these figures, the increase of $\dot{S}_{T,a}$ has continued with high growing after $T_\infty = 15$ °C. Also in all figures, the value for $\dot{S}_{T,a}$ is minimized when the value for arc limits to 0.5. Fig. 11 shows the variation of the total entropy generation vs. aspect ratio (L/H), for different ambient temperatures ($T_\infty = 10, 15, 17$ °C). This work was conducted for heat flux of $q = 650\,\text{W/m}^2$, $T_G = 23$ °C and arc $= 0.5$. It can be observed that the total entropy generation decreases in function of the aspect ratio and increases in function of the ambient temperature.

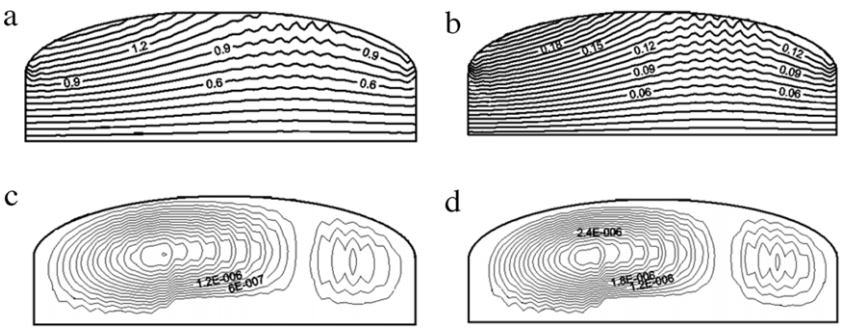

Fig. 9. Isotherms (a–b) and streamlines (c–d) for greenhouse (with $L/H = 3$, arc $= 0.5$ and $T_G = 23$ °C), in two different ambient temperatures: (1) $T_\infty = 22$ °C (left figures) and (2) $T_\infty = 10$ °C (right figures).

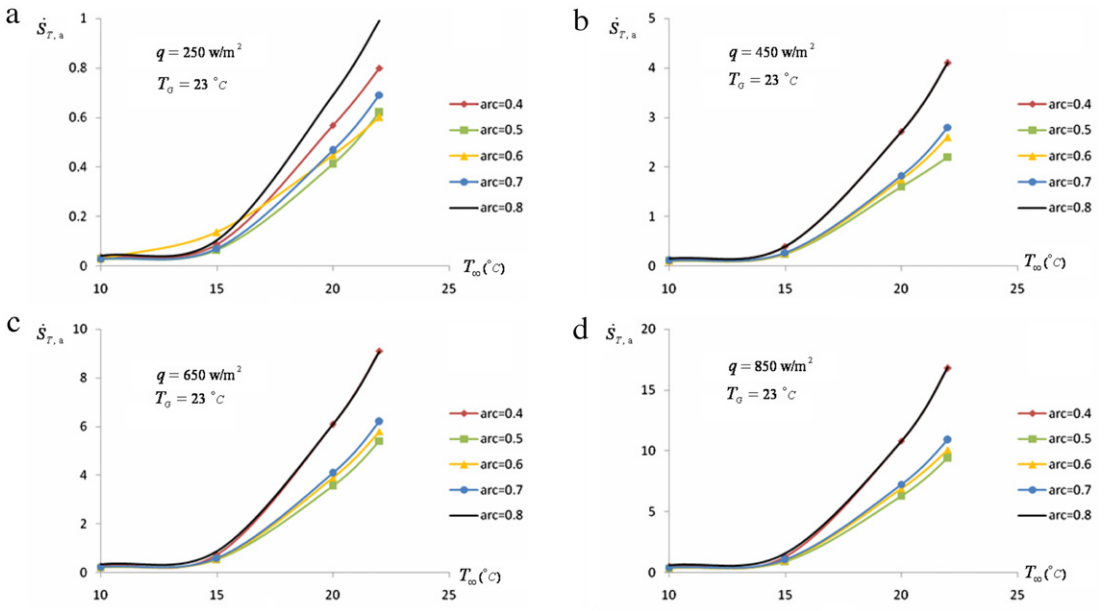

Fig. 10. The variation of the total entropy generation $\dot{S}_{T,a}$ vs. the ambient temperature T_∞, for different arc values (arc $= 0.4, 0.5, 0.6, 0.7, 0.8$), when $T_G = 23$ °C.

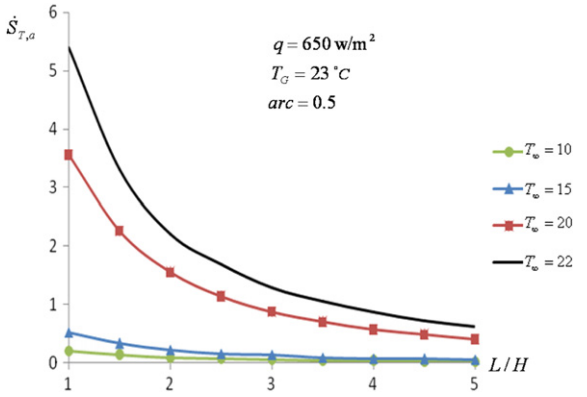

Fig. 11. The variation of the total entropy generation vs. aspect ratio (L/H), for different ambient temperatures ($T_\infty = 10, 15, 20, 22$ °C), when $T_G = 23$ °C.

5.2.3. The simulation and the comparison results for the one-sided roof

Velocity fields have been shown in Figs. 12. Two figures have been sketched (with $L/H = 1$ and $\tan\alpha = 0.5$), in two different ambient temperatures: (1) $T_\infty = 22$ °C (Fig. 12a) and (2) $T_\infty = 10$ °C (Fig. 12b). It is revealed that, in Fig. 12a,

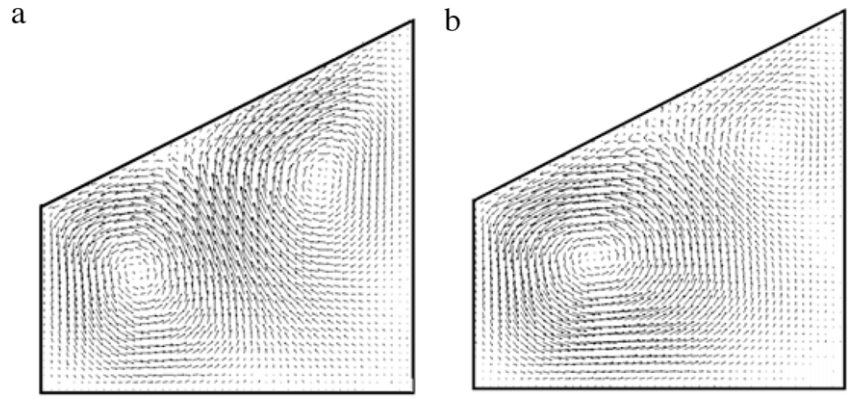

Fig. 12. Velocity fields for one-sided roof greenhouse (with $L/H = 1$, $\tan\alpha = 0.5$ and $T_G = 23$ °C), in two different ambient temperatures: (1) $T_\infty = 22$ °C (a) and (2) $T_\infty = 10$ °C (b).

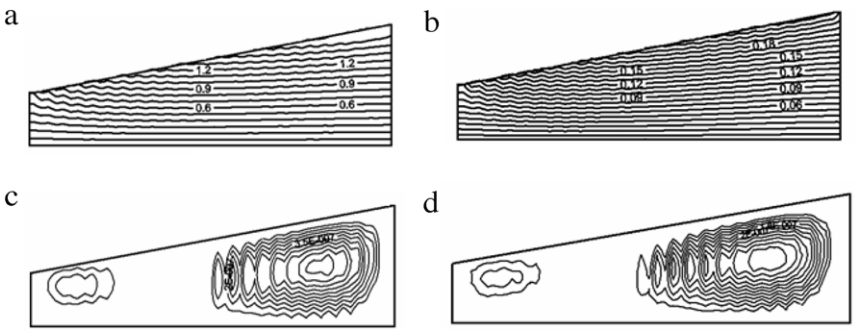

Fig. 13. Isotherms (a–b) and streamlines (c–d) for greenhouse (with $L/H = 3$, $\tan\alpha = 0.5$ and $T_G = 23$ °C), in two different ambient temperatures: (1) $T_\infty = 22$ °C (left figures) and (2) $T_\infty = 10$ °C (right figures).

two approximately equal circulations (with opposite spin) are formed due to the free convection heat transfer mechanism. According to Fig. 12b, with decreasing ambient temperature, the left circulation penetrates into the right circulation.

For aspect ratio equal to 3 ($L/H = 3$) the isotherms and their stream lines have been shown in Fig. 13a–d. According to stream lines, it is revealed that two main circulations, one the larger circulation cell on the right and the other the weaker circulation cell on the left, are formed in the greenhouse.

Fig. 14a–d, show the variation of the total entropy generation $\dot{S}_{T,a}$ vs. the ambient temperature T_∞, for different slope angles ($\tan\alpha = 0.5, 0.6, 0.7, 0.8$). In all figures the value of ground temperature is constant ($T_G = 23$ °C). It is seen that with increasing T_∞, the $\dot{S}_{T,a}$ increases. As shown in these figures, the increase of $\dot{S}_{T,a}$ has continued with high growing after $T_\infty = 15$ °C. Also in all figures the value for $\dot{S}_{T,a}$ is minimized when $\tan\alpha = 0.5$.

Fig. 15 shows the variation of the total entropy generation vs. aspect ratio (L/H), for different ambient temperatures ($T_\infty = 10, 15, 20, 22$ °C). This work was conducted for heat flux of $q = 650$ W/m^2, $T_G = 23$ °C and $\tan\alpha = 0.5$. It can be observed that the total entropy generation decreases in function of the aspect ratio and increases as function of the ambient temperature.

In this work, we compared the entropy generations between arc-roof and one-sided roof greenhouses (Fig. 16). According to this figure curves, one can see that the one-sided roof greenhouse has the minimum entropy generation in comparison with the arc-roof greenhouse.

As shown in Fig. 17, we sketched temperature distribution of the inside arc-roof greenhouse (in the case of arc = 0.5) at $X = 0.5$, for different heat flux values, when $T_G = 23$ °C and $T_\infty = 20$ °C. According to all curves, it is seen that, the values of temperatures at the neighboring roof are maximized.

6. Conclusions

In this paper, a FORTRAN code was developed using the cell-centered finite-volume method for solving the incompressible natural convection flow within both the arc-roof and one-sided roof enclosures. An explicit fourth-order Runge–Kutta integration algorithm was applied to find the steady state solutions. Also an artificial compressibility technique was applied to couple the continuity to the momentum equations. The enclosures were assumed like two-dimensional

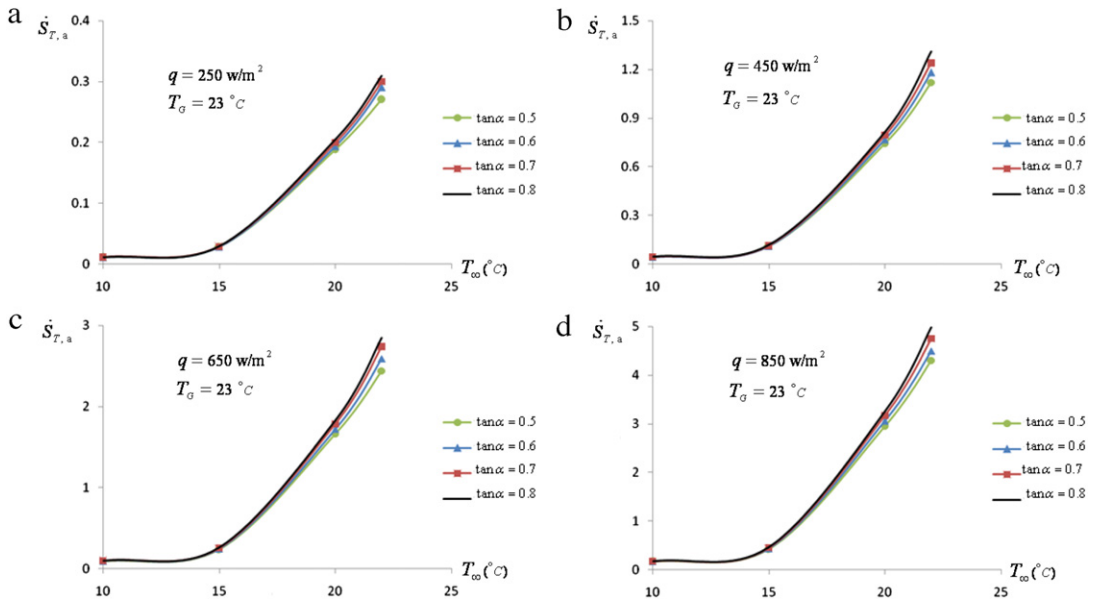

Fig. 14. The variation of the total entropy generation $\dot{S}_{T,a}$ vs. the ambient temperature T_∞, for different slope angles ($\tan\alpha = 0.5, 0.6, 0.7, 0.8$), when $T_G = 23$ °C.

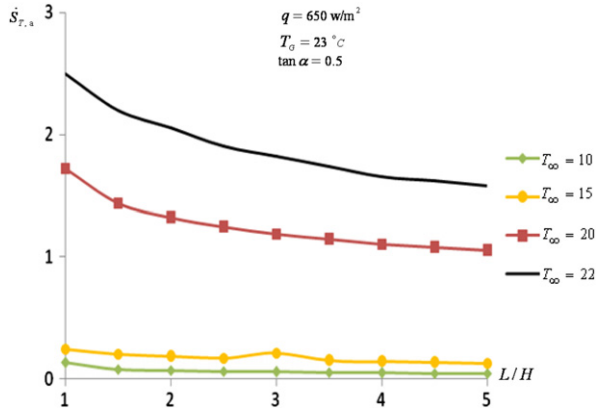

Fig. 15. The variation of the total entropy generation vs. aspect ratio (L/H), for different ambient temperatures ($T_\infty = 10, 15, 20, 22$ °C), when $T_G = 23$ °C.

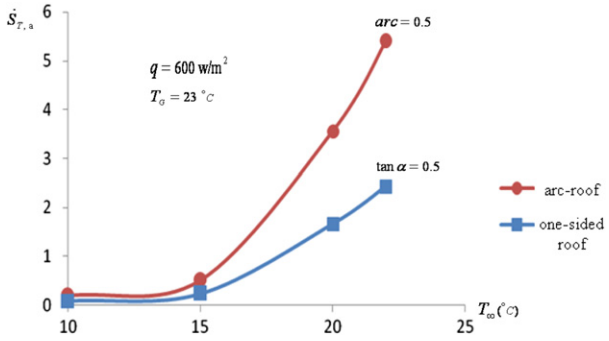

Fig. 16. Entropy generation comparison between the arc-roof and the one-sided roof greenhouses.

enclosures with the laminar free convection of air flow into them. The discretization of the viscous and thermal conduction terms were very simplified using the enhanced scheme similar to the flux averaging in the convective term. In this enhanced method, the terms of the volumetric entropy generation in flow due to the heat transfer and the fluid friction are initially

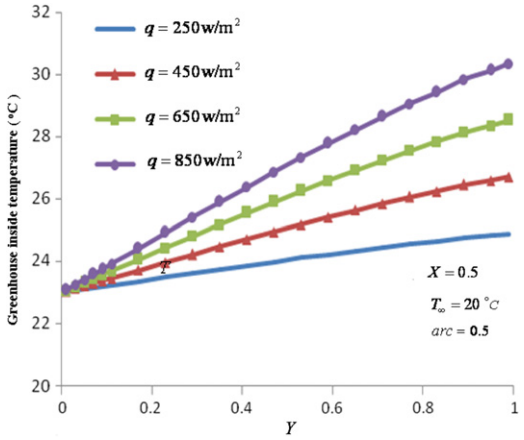

Fig. 17. Temperature distribution of the inside arc-roof greenhouse (in the case of arc $= 0.5$) at $X = 0.5$, for different heat flux values, when $T_G = 23$ °C and $T_\infty = 20$ °C.

considered as dependent variables, and then obtained directly after the each time step within the time marching processes. The some important results are as follows.

- ✓ The good convergence speed has been obtained for artificial compressibility as $\beta = 300$.
- ✓ In the arc-roof enclosure, the value for $\dot{S}_{T,a}$ is minimized when the value for arc limits to 0.5.
- ✓ In the one-sided roof enclosure, the value for $\dot{S}_{T,a}$ is minimized when the value for slope angle limits to $\tan\alpha = 0.5$.
- ✓ In both the arc-roof and one-sided roof enclosures, the total entropy generation $\dot{S}_{T,a}$ decreases in function of the aspect ratio and increases as function of the ambient temperature.
- ✓ In equal conditions, the one-sided roof enclosure has the minimum entropy generation in comparison with the arc-roof enclosure.

References

[1] B.M. Ziapour, R. Dehnavi, Finite-volume method for solving the entropy generation due to air natural convection in Γ-shaped enclosure with circular corners, Math. Comput. Modelling 54 (2011) 1286–1299.
[2] D.C. Oliveski, M.H. Macagnan, J.B. Copetti, Entropy generation and natural convection in rectangular cavities, Appl. Therm. Eng. 29 (2009) 1417–1425.
[3] I. Dagtekin, H.F. Oztop, A. Bahloul, Entropy generation for natural convection in Γ-shaped enclosures, Int. Commun. Heat Mass Transfer 34 (2007) 502–510.
[4] Y.L. He, W.Q. Tao, T.S. Zhao, Z.Q. Chen, Natural convection in a tilted long cylindrical envelope with lateral adiabatic surface, part 1: theoretical modeling, Numer Heat Transfer 44 (2003) 375–397.
[5] G. Barakos, E. Mitsoulis, Natural convection flow in a square cavity revisited: laminar and turbulent models with wall function, Int. J. Numer. Methods Fluids 18 (1994) 695–719.
[6] D.K. Edwards, I. Catton, Prediction of heat transfer by natural convection in closed cylinders heated from below, Int. J. Heat Mass Transfer 12 (1969) 25–30.
[7] D.K. Fidaros, C.A. Baxevanou, T. Bartzanas, C. Kittas, Numerical simulation of thermal behavior of a ventilated arc greenhouse during a solar day, Renew. Energy 35 (2010) 1380–1386.
[8] G. Gan, CFD modelling of transparent bubble cavity envelopes for energy efficient greenhouses, Build. Env. 44 (2009) 2486–2500.
[9] A.M. Abdel-Ghany, I.M. Al-Helal, Solar energy utilization by a greenhouse: general relations, Renew. Energy 36 (2011) 189–196.
[10] W. Chen, W. Liu, B. Liu, Numerical and experimental analysis of heat and moisture content transfer in a lean-to greenhouse, Energy Build. 38 (2006) 99–104.
[11] W. Chen, W. Liu, Numerical simulation of the airflow and temperature distribution in a lean-to greenhouse, Renew. Energy 31 (2006) 517–535.
[12] P.K. Sharma, G.N. Tiwari, V.P.S. Sorayan, Temperature distribution in different zones of the micro-climate of a greenhouse: a dynamic model, Energy Convers. Manage. 40 (1999) 335–348.
[13] I. Impron, S. Hemming, G.P.A. Bot, Simple greenhouse climate model as a design tool for greenhouses in tropical lowland, Biosyst. Eng. 98 (2007) 79–89.
[14] H. Fatnassi, T. Boulard, C. Poncet, M. Chave, Optimisation of greenhouse insect screening with computational fluid dynamics, Biosyst. Eng. 93 (2006) 301–312.
[15] V.P. Sethi, On the selection of shape and orientation of a greenhouse: thermal modeling and experimental validation, Sol. Energy 83 (2009) 21–38.
[16] M. Djevic, A. Dimitrijevic, Energy consumption for different greenhouse constructions, Energy 34 (2009) 1325–1331.
[17] M. Bidi, M.R.H. Nobari, M.S. Avval, A numerical evaluation of combustion in porous media by EGM (Entropy Generation Minimization), Energy 35 (2010) 3483–3500.
[18] A. Bejan, Entropy generation minimization: the new thermodynamics of finite-size devices and finite-time processes, J. Appl. Phys. 79 (1996) 1191–1218.
[19] Z.H. Xie, L.G. Chen, F.R. Sun, Geometry optimization of T-shaped cavities according to constructal theory, Math. Comput. Modelling 52 (2010) 1538–1546.
[20] A. Jameson, D. Mavriplis, Finite volume solution of the two-dimensional Euler equations on a regular triangular mesh, AIAA J. 24 (1986) 611–618.
[21] V. Esfahanian, P. Akbarzadeh, The Jameson's numerical method for solving the incompressible viscous and inviscid flows by means of artificial compressibility and preconditioning method, Appl. Math. Comput. 206 (2008) 651–661.
[22] A.J. Chorin, A numerical method for solving incompressible viscous flow problems, J. Comput. Phys. 2 (1967) 12–26.
[23] A.J. Chorin, A numerical method for solving incompressible viscous flow problems, J. Comput. Phys. 112 (1997) 118–125.
[24] P.A. Madsen, H.A. Schäffer, A discussion of artificial compressibility, Coastal Eng. 53 (2006) 93–98.
[25] F. Bassi, A. Crivellini, D.A. Pietro, S. Rebay, An artificial compressibility flux for the discontinuous Galerkin solution of the incompressible Navier–Stokes equations, J. Comput. Phys. 218 (2006) 794–815.
[26] M. Famouri, K. Hooman, Entropy generation for natural convection by heated partitions in a cavity, Int. Commun. Heat Mass Transfer 35 (2008) 492–502.